

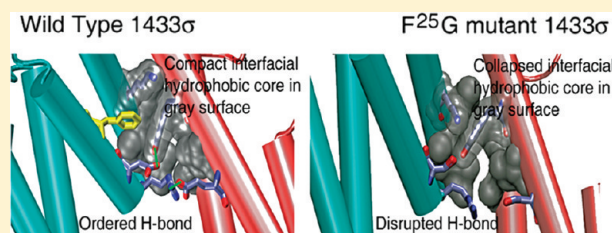
Critical Residue That Promotes Protein Dimerization: A Story of Partially Exposed Phe²⁵ in 14-3-3 σ

Jing-Yuan Liu,^{†,*} Zhaomin Li,[†] Huian Li,[‡] and Jian-Ting Zhang^{†,§,*}

[†]Department of Pharmacology and Toxicology, [‡]University Information Technology Services, and [§]IU Simon Cancer Center, Indiana University School of Medicine, Indianapolis, Indiana 46202, United States

 Supporting Information

ABSTRACT: Many proteins exist and function as oligomers. While hydrophobic interactions have been recognized as the major driving force for oligomerization, detailed molecular mechanisms for the assembly are unknown. Here, we used 14-3-3 σ as a model protein and investigated the role of hydrophobic residues at the dimeric interface using MD simulations and coimmunoprecipitations. We found that a half-exposed and half-buried residue in the interface, Phe²⁵, plays a more important role in promoting homodimerization than the hydrophobic core residues by organizing both favorable hydrophobic and hydrophilic interactions. Phe²⁵ is critical in packing and stabilizing hydrophobic core residues. We conclude that the structural stability of hydrophobic cores is critical for a stable homodimer complex and this stable property can be bestowed by residues outside of hydrophobic core. The important organizing activity of Phe²⁵ for homodimerization of 14-3-3 σ originates from its unique physical location, rigidity, size, and hydrophobicity. Thus, hydrophobic residues that are not deeply buried at the oligomeric interface may play important but different roles from the buried core residues and they may promote oligomerization by organizing co-operativity of core and other residues for favorable hydrophobic and electrostatic interactions.



INTRODUCTION

Protein–protein interactions are important for biological functions, and alterations in protein–protein interaction events can cause diseases such as cancer and diabetes.^{1,2} However, how proteins recognize each other and form stable complexes is not fully understood. It is often difficult to differentiate specific protein–protein interactions found in protein complexes from the non-specific interactions resulting from crystal packing in crystallography.^{3–5} Although hydrophobic interactions have been recognized as the major driving force in protein–protein interactions,^{6–9} the detailed molecular mechanism and the assembly process of protein oligomerization is largely unknown. Interfacial residues that are deeply buried in the interface and often hydrophobic are thought to be important and mutation of these so-called hot-spot residues compromises the affinity between associating subunits.^{10,11}

In this report, we studied protein homodimerization, the simplest form of protein–protein interaction between two identical chains, by using 14-3-3 σ as a model protein. 14-3-3 σ is a member of the highly conserved 14-3-3 protein family found in all eukaryotic organisms and it is unique in strictly forming only homodimers¹² while the other human family members, 14-3-3 β , γ , ε , ζ , η , and τ , can form both homo- and heterodimers.^{13–17} By virtually mutating three interfacial hydrophobic residues (Leu¹², Phe²⁵, and Tyr⁸⁴) and performing molecular dynamics (MD) simulations and analyses of mm-GBSA free energy of both wild type and mutant 14-3-3 σ , we show that although mutation of the two deeply buried interfacial core residues Tyr⁸⁴ and Leu¹² into Gly significantly reduces the binding affinity between the two subunits, mutation of the

half-exposed Phe²⁵ to Gly is most detrimental, which is confirmed by coimmunoprecipitation in combination with Western blot analysis. F²⁵G has the most unstable and loosely packed interfacial cores that had highest water exchange rate. Phe²⁵ with its unique physical location and properties plays an important role in promoting both hydrophobic and hydrophilic interactions favorable for homodimerization.

MATERIALS AND METHODS

Molecular Modeling and MD Simulation. The crystal structure of 14-3-3 σ with pdb code 1YWT from the protein databank was used as the template structure. Missing loops were modeled by MOE with the homology modeling module. Mutations of specific residues were introduced with the UCSF Chimera swapaa function. FF03 parameters and hydrogen atoms were assigned to the protein by leap module of AMBER9.

MD simulations of wild-type and mutant 14-3-3 σ dimers were carried out using the AMBER9 package. All dimers were solvated in a 84 × 103 × 67 Å rectangular box. An appropriate number of counterions were added to neutralize each system. Particle Mesh Ewald (PME) was employed to calculate the long-range electrostatic interactions and the nonbonded cutoff was set to 8.0 Å.

Each system was equilibrated by a four-step protocol prior to production MD simulation. First, the solvated structures were

Received: May 12, 2011

Published: August 28, 2011

minimized with a restraint of 500 kcal/mol·Å² applied to the proteins. The restraint was then removed and the energy of the whole system was minimized. In these two steps, 500 and 1000 steps of steepest descent minimization followed by 500 and 1500 steps of conjugate gradient minimization were applied, respectively. Each system was then heated up from 0 to 300 K gradually over a duration of 20 ps controlled by Langevin temperature equilibration scheme with a collision frequency of 1.0 ps⁻¹. The system was then equilibrated at 300 K for 100 ps using constant volume periodic boundaries. Weak position restraint of 10 kcal/mol·Å² to the protein complexes and SHAKE procedure to all bonds containing hydrogen atoms were applied to each system in the above steps. Restraint to the protein was removed in the final 1 ns equilibrium run. The same conditions of the final equilibration step were used for production MD simulation of 20 ns.

A total of 500 snapshots were collected from the production trajectory for MM-GBSA free energy calculations. The structures of the two individual chains were extracted from the snapshots of each protein dimer and were assigned as receptor and ligand, respectively. The binding free energies were then computed by taking the difference between the MM-GBSA free energy of the complex and that of the summation of the receptor and ligand chains. The electrostatic contribution to the solvation free energy was determined by GBSA in AMBER9. The grid size was set as 0.5 Å, and the dielectric constants for the solute and solvent were set as 1 and 80, respectively. For each trajectory, RMSD and dihedral angles were calculated for each 10 ps frame by the rms and dihedral commands of the AMBER9 ptraj module, respectively. RMSF of interfacial core residues were calculated by the atomicfluct command of ptraj.

Total surface areas and buried dimeric interface areas were calculated by areaimol of the CCP4 package.¹⁸ To monitor the water exchange rate at the interfacial core of the dimeric interface, interfacial core residues that have more than 80% solvent accessible area buried in the dimeric interface were chosen for each subarea. The center of mass of these residues was determined for each frame and a sphere of 6 Å in radius was drawn from this center. Water molecules that fell into the sphere during the simulation were monitored and their residue IDs were recorded by the VMD program. Then, the water molecules from every 20 frames (representing a 200 ps timespan) were pooled and compared with that from the previous 20 frames. Water molecules with residue IDs that existed in the current 20 frames but did not appear in the previous 20 frames were considered water molecules that moved in during the current 200 ps timespan. Water molecules with residue IDs found in the current 20 frames but did not show up again in the next 20 frames were considered water molecules that moved out during this 200 ps timespan.

Engineering, Expression, and Coimmunoprecipitation of Mutant 14-3-3σ. Tagged 14-3-3σ mutants were engineered using QuickChange Site-Directed Mutagenesis Kits as previously described.¹⁹ The cDNA templates encoding Flag- or Myc-tagged 14-3-3σ were from a previous study²⁰ and paired primers are shown in Supporting Information Table S1. All 14-3-3σ mutants were finally engineered into pcDNA3.1(+) (Invitrogen) and confirmed by double strand DNA sequencing.

The pancreatic cancer cell line MiaPaCa-2 lacking endogenous 14-3-3σ²⁰ was maintained in DMEM supplemented with 10% fetal bovine serum, 2.5% donor equine serum (HyClone), and 1% penicillin/streptomycin mixture. cDNA constructs encoding Flag-tagged 14-3-3σ were transfected into MiaPaCa-2 cells using Lipofectamine (Invitrogen) and stable clones were selected using

1 mg/mL G418 (Invitrogen) as previously described.^{21,22} The stable clones were maintained in complete DMEM supplemented with 200 µg/mL G418.

Co-immunoprecipitation was performed as previously described.²³ Briefly, the stable cell lines expressing Flag-tagged wild-type and mutant 14-3-3σ were seeded and cultured overnight followed by transient transfection with Myc-tagged wild-type or mutant 14-3-3σ constructs using Lipofectamine. The cells were cultured for 48 h before harvest and preparation of cell lysates in TNN buffer [50 mM Tris·HCl, pH 7.4, 150 mM NaCl, 5% NP-40, 20 mM EDTA, 50 mM NaF, 1 mM Na₃VO₃, 1 mM PMSF, 1 mM DTT] followed by incubation with normal mouse IgG for 1 h at 4 °C, additional incubation for 1 h at 4 °C in the presence protein G-agarose beads, and centrifugation to remove nonspecifically bound materials. The supernatant was then incubated with anti-FLAG antibody (Sigma) at 4 °C for 3 h before mixing with protein G-agarose slurry. The mixtures were further incubated at 4 °C overnight followed by centrifugation to collect precipitates which were then washed five times before being subjected to Western blot analysis using anti-Myc or anti-FLAG antibodies.

RESULTS

Analysis of Native X-ray Structure. There are two crystal structures of 14-3-3σ in the RCSB Protein Data Bank: a non-liganded apoprotein at a resolution of 2.8 Å (PDB code: 1YZS)¹⁵ and a phospho-peptide complex at a resolution of 2.4 Å (PDB code: 1YWT)¹². These two structures are nearly identical with a root-mean-square deviation (RMSD) of 0.8 Å when 198 C-α atom pairs were aligned. Consequently, the crystal structure of 1YWT was chosen for this study due to its higher resolution.

The overall structure of 14-3-3σ is composed of two layers of helices. Helices A, B, C, D, E, and F from both subunits form the bottom layer while helices G, H, and I from each subunit reside on the top on each side (Figure 1A). The two phospho-peptide ligands, which are not a focus of this work and not included in our MD simulations, are located in the cleft formed by helices C and E in bottom layer and helices G and I in top layer (Figure 1A). The two subunits of 14-3-3σ dimerize through interactions between helices A and B of one subunit and helices C and D of the other and vice versa. This mode of interaction creates an aperture that divides the dimeric interface into two subareas, I and II (Figure 1B). These two subareas are structurally similar and are related by the pseudo-2-fold symmetry of the protein. The total buried dimeric interface in 14-3-3σ is 980 Å², which is about 4.5% of the total solvent accessible area of a dimer. In each subarea, interfacial core residues Lys⁹, Leu¹², Ala¹³, and Ala¹⁶ of one subunit interact with interfacial core residues Ala⁵⁸, Leu⁶², Tyr⁸⁴, and Val⁸⁸ of the opposing subunit. These residues are defined as the interfacial core residues because they are located in the center of each subarea and all have >80% of their solvent accessible area buried in the dimeric interface (Table 1). On the basis of the composition of the residues, the chemical property of the interfacial core is hydrophobic. The top two residues, Tyr⁸⁴ and Leu¹² have 99% and 96% of their solvent accessible area buried in the dimeric interface, respectively, and provide the most buried surface area (120 and 88 Å², respectively). Phe²⁵, which is not conserved in 14-3-3 protein family but unique to the σ isoform, is not located in the interfacial core of the interface (Figure 1B). It has only ~50% of its solvent accessible area buried in the dimeric interface. The absolute interacting surface area it provides is 25 Å²

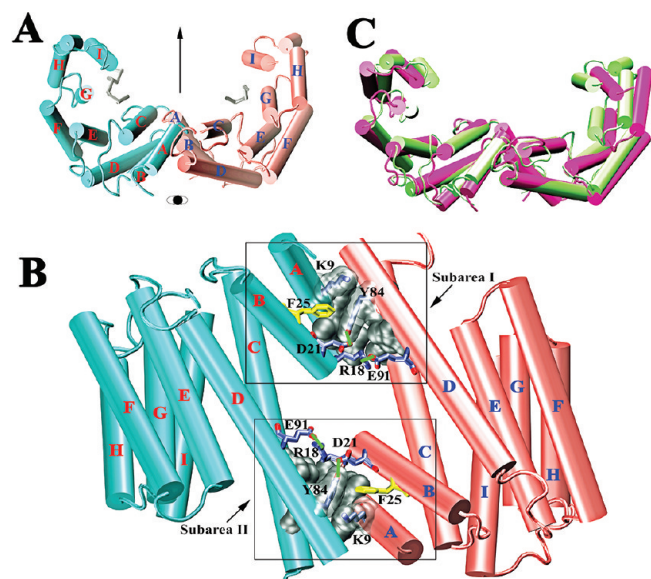


Figure 1. Initial and simulated structures of wild-type 14-3-3 σ . (A) and (B) Initial structure of wild type 14-3-3 σ viewed perpendicular (A) or parallel (B) to its pseudo-2-fold axis. The two identical chains of a dimer are shown in cyan and pink, respectively. Helices are shown as labeled cylinders. Pseudo-2-fold axis is shown by an arrow. The two phosphopeptides which are not included in our calculation are shown as stick symbols in gray in panel A. The eye sign in panel A indicates the view from which is seen in panel B. Interfacial core residues that are deeply buried in the dimeric interface are shown by their molecular surface in gray and the two polar residues, Lys⁹ and Tyr⁸⁴, are shown by their molecular surface in transparency and by stick representation. Phe²⁵ is shown in yellow. Residues that form strong hydrogen bonds across the dimeric interface are shown by their atom types. Hydrogen bonds are indicated by green lines. (C) Superposition of the average structure of the 20-ns simulation (in magenta) and the initial structure (in green) of the wild-type 14-3-3 σ dimer. The superimposed structures were positioned similarly to that in panel A.

which ranks seventh in all 13 hydrophobic interfacial residues (Table 1).

In addition to hydrophobic interactions, there are 12 hydrogen bonds between the two subunits. Strong hydrogen bonds with distances lower than 3 Å in both subareas are observed between Arg¹⁸ and Glu⁹¹, and between Asp²¹ and Tyr⁸⁴ (Figure 1B).

The Open/Close Motion in apo-14-3-3 σ Homodimer. To better understand the dynamic properties of the protein dimeric interface and the roles of hydrophobic residues in dimer formation, we virtually mutated the top two ranked residues, Tyr⁸⁴ and Leu¹², as well as the unique Phe²⁵ into Gly individually and created L¹²G, F²⁵G, and Y⁸⁴G mutants and performed 20-ns MD simulations for wild-type and mutant 14-3-3 σ . Gly was chosen as an ultimate mutated residue because it does not carry any hydrophobic side chains. The average structures from MD simulations were calculated and aligned with the initial structure. Figure 1C shows the aligned structures of wild type 14-3-3 σ . It appears that the average simulated structure of wild type 14-3-3 σ represents a more open conformation in which bottom helices A, B, C, and D that engage in dimerization are in near complete alignment with that of the initial structure, while top helices G, H, and I of the two subunits in the average simulated structures are located slightly further away from each other and cannot be aligned with the initial structure. The average simulated structures of L¹²G,

Table 1. Residues and Their Buried Surface Areas Found at the Dimeric Interface

hydrophobic residues ^a	buried surface area ^b	polar/charged residues ^a	buried surface area ^b
TYR84	120(99)	ARG18	110(76)
LEU12	88(96)	GLU80	81(63)
ALA16	58(91)	LYS9	70(83)
VAL61	44(54)	GLN15	44(30)
ILE65	38(36)	ASP21	39(66)
ALA58	36(100)	GLU83	28(21)
PHE25	25(53)	LYS87	26(24)
LEU62	25(100)	SER5	25(63)
VAL81	24(42)	GLU91	24(26)
VAL88	14(100)	GLN8	23(25)
ALA13	9(100)	GLN55	11(55)
GLY54	8(19)	GLU20	8(5)
MET1	2(2)		

^aResidues are ranked by their buried surface areas at the dimeric interface each residue provides. ^bBuried surface areas are given in Å² and the number in parentheses is the percentage of solvent accessible area that becomes buried upon dimerization.

F²⁵G, and Y⁸⁴G mutants are the same as that of wild-type in that the top helices of the two subunits moved away from each other compared with the initial structure.

To further investigate the motion of top helices G, H, and I during simulation (Figure 1C), overall conformational dynamics and changes of the 20-ns trajectories of wild-type and mutant 14-3-3 σ were examined and illustrated by RMSD of main chain atoms (Figure 2A, Table 2). Overall RMSDs of wild-type and mutant proteins all reach 6 Å, indicating large conformational changes during simulations. Examination of the trajectories revealed that helices G, H, and I in wild-type and mutants are mobile and 14-3-3 σ transits between closed and open conformations. This conformational transition can be easily detected by change in distance between the center of mass of the two sets of helices G, H and I (Figure 2B, Table 2). The larger value indicates a more open conformation while a smaller value indicates a more closed one.

In contrast, the main chain RMSDs of bottom helices A, B, C, and D (residues 1 to 107) that are engaged in dimerization are below 3 Å in wild-type and mutant proteins (Figure 2C, Table 2), suggesting that they are structurally stable. The distances between the center of mass of the two sets of bottom helices A, B, C, and D remain constant during simulation, also reflecting the stability of these helices (Figure 2D, Table 2). Thus, relative to top helices G, H, and I that are involved in ligand binding, bottom helices A, B, C, and D that are involved in dimerization are structurally stable. Furthermore, L¹²G, F²⁵G, and Y⁸⁴G mutations do not appear to have major effects on overall conformational changes of helices G, H, and I.

Effects of Leu¹², Phe²⁵, or Tyr⁸⁴ Mutation on Secondary Structures of 14-3-3 σ . Since Gly can be a helix breaker, we next investigated whether L¹²G, F²⁵G, and Y⁸⁴G mutations possibly alter the main chain conformation of 14-3-3 σ by examining the occupancy of residues 7 to 107 in α -helices during the 20-ns simulations. The residues in helices A to D of the mutants are mostly maintained in α -helices during the 20-ns simulations, similar to the wild type protein (Supporting Information Figure S1).

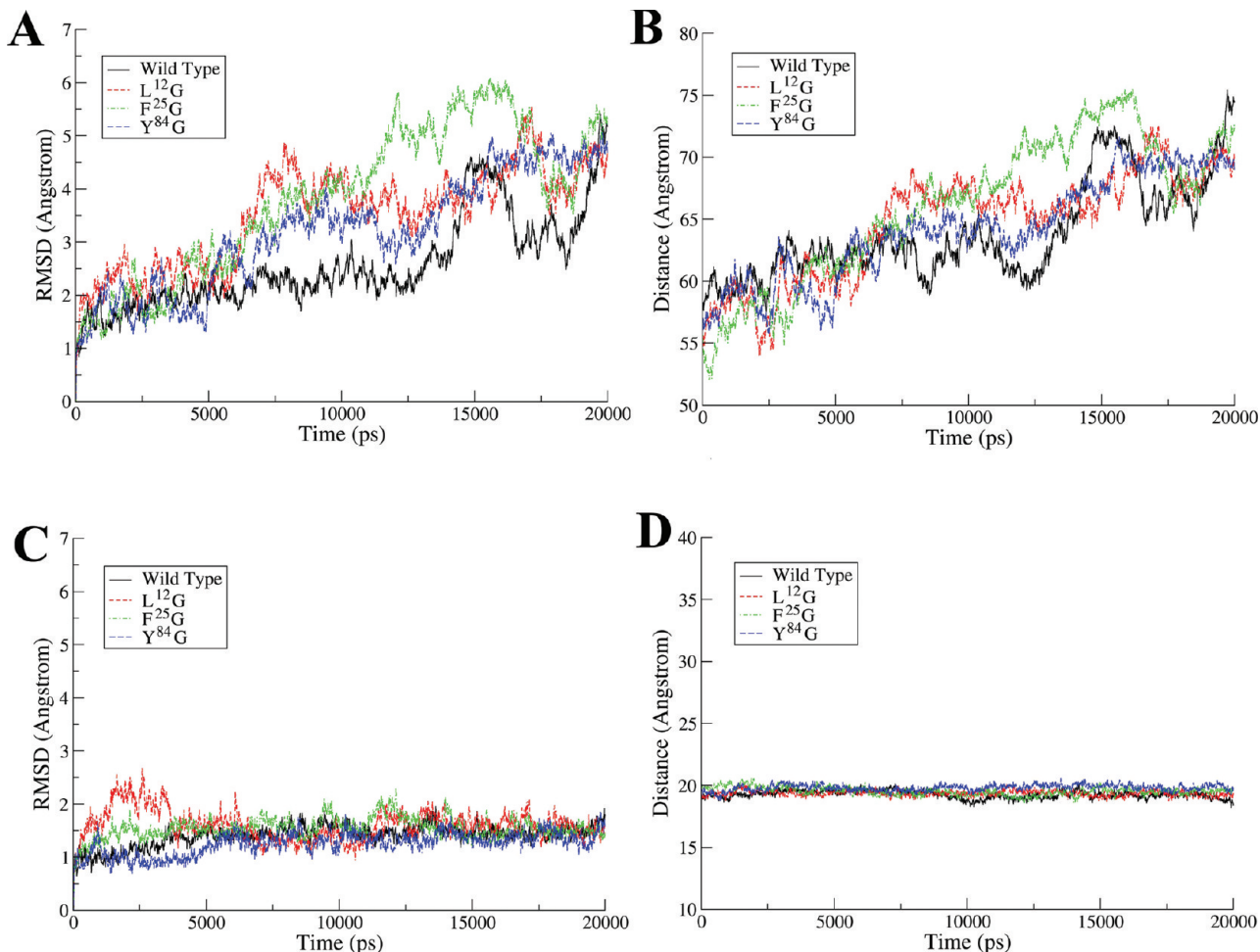


Figure 2. (A) and (C) Main chain RMSD of overall protein (A) and of residues 1 to 107 (C) from the first frame throughout MD simulations. (B) and (D) Distance between the center of mass of the two sets of helices G, H, and I on the two chains (B) and the two sets of helices A, B, C, and D on the two chains (D) during the simulations.

Therefore, none of the mutations cause any major effects on the integrity of secondary structures of 14-3-3 σ .

Effects of Leu¹², Phe²⁵, or Tyr⁸⁴ Mutation on Dimer Formation. To determine how each mutation affects 14-3-3 σ dimerization, binding free energies between the two associating subunits were calculated for wild type and L¹²G, F²⁵G, and Y⁸⁴G mutants using the GBSA method.²⁴ The binding free energy is computed by taking the difference between the mm-GBSA free energy of the complex with that of the ligand and receptor: $\Delta G_{\text{bind}} = G_{\text{complex}} - G_{\text{receptor}} - G_{\text{ligand}}$ where $G = G^{\text{solute}} + G^{\text{solvent}}$. The G^{solute} term for each system can be obtained by $G^{\text{solute}} = E - TS$. E represents an average of energies obtained from MD simulation and is the sum of the following 3 terms: “non-bonded electrostatic energy + 1,4-electrostatic energy” (E^{ele}); “non-bonded van der Waals energy + 1,4-van der Waals energy” (E^{vdw}) and “bond, angle, dihedral energies” (E^{int}). S is the entropy contribution that is omitted from our calculation because the purpose of this work is to compare the effect of each mutation on dimerization rather than to calculate absolute binding free energy. The G^{solvent} term can be obtained by $G^{\text{solvent}} = G^{\text{es}} + G^{\text{nes}}$. G^{es} is the electrostatic contribution that is obtained by the GB method, and G^{nes} is the nonelectrostatic contribution and is proportional to the solvent-accessible surface area of the molecule. As the entropy term is not included in this study, the calculated

total binding free energy (ΔG_{bind}) is only composed of the E and G^{solvent} terms.

As shown in Table 3, wild-type 14-3-3 σ has the most favorable calculated total binding free energy followed by L¹²G and Y⁸⁴G mutants. Surprisingly, F²⁵G has the most unfavorable calculated total binding free energy although Phe²⁵ is not deeply buried in the dimeric interface. Considering the omission of the entropy term, which is always unfavorable, F²⁵G may have little dimerization activity.

In vacuum, none of the wild type and mutant dimers have favorable electrostatic interaction energy. L¹²G and Y⁸⁴G have more favorable electrostatic free energy in vacuum than the wild type. This term is significantly less favorable in F²⁵G, which is the major cause for the unfavorable total binding free energy. In all dimers, the contribution from van der Waals forces and solvation effects reversed the unfavorable electrostatic energy terms in vacuum.

To validate the above findings, we tested the effect of L¹²G, F²⁵G, and Y⁸⁴G mutations on 14-3-3 σ dimerization using coimmunoprecipitation and Western blot analyses. For this purpose, Myc-tagged wild type and mutant 14-3-3 σ were transiently transfected into stable cell lines expressing Flag-tagged wild type or mutant proteins for coexpression, followed by immunoprecipitation using Flag antibody and Western blot analyses using Flag and Myc antibodies. As shown in Figure 3A, the

Table 2. Average RMSDs, Distances, and Dihedral Angles

properties	WT	$L^{12}G$	$F^{25}G$	$Y^{84}G$
overall main chain RMSD \pm S.D. ^a	2.55 ± 0.87	3.52 ± 0.92	3.01 ± 1.39	3.20 ± 1.07
main chain RMSD \pm S.D. ^a (Res. 1–107)	1.40 ± 0.20	0.70 ± 0.12	1.55 ± 0.20	1.26 ± 0.21
distance ^b between helices ABCD (Å)	19.27 ± 0.31	19.37 ± 0.22	19.54 ± 0.33	19.81 ± 0.26
distance ^b between helices GHI (Å)	63.85 ± 3.87	64.70 ± 4.29	65.97 ± 5.76	64.18 ± 4.08
all atoms RMSD of hydrophobic core residues \pm S.D.	subarea I	0.64 ± 0.08	0.70 ± 0.12	1.08 ± 0.14
χ^1 ^c of Lys ⁹ \pm S.D.	subarea II	$0.98^d \pm 0.07$	0.73 ± 0.11	1.16 ± 0.21
	subunit I	163 ± 12	147 ± 35	66 ± 13
	subunit II	165 ± 10	155 ± 37	63 ± 14
χ^1 ^c of Phe ²⁵ \pm S.D.	subunit I	167 ± 8	168 ± 9	168 ± 8
	subunit II	167 ± 8	166 ± 8	168 ± 8
χ^2 ^c of Phe ²⁵ \pm S.D.	subunit I	126 ± 10	134 ± 11	131 ± 9
	subunit II	131 ± 10	130 ± 10	129 ± 10
χ^1 ^c of Tyr ⁸⁴ \pm S.D.	subunit I	189 ± 7	186 ± 7	196 ± 13
	subunit II	189 ± 7	184 ± 7	190 ± 10
χ^2 ^c of Tyr ⁸⁴ \pm S.D.	subunit I	$54^e \pm 14$	50 ± 12	64 ± 34
	subunit II	48 ± 15	54 ± 12	44 ± 27

^a S.D. = standard deviation. ^b RMSDs and distances are in angstrom. ^c Dihedrals are in degrees. ^d Data from 600 ps to 2 ns were used. ^e Data from 200 ps to 2 ns were used.

Table 3. Calculated Binding Free Energies and Energy Components of Wild-Type and Mutant 14-3-3 σ ^a

	ΔE_{solute}			ΔE_{solv}		
	ΔE_{ele}	ΔE_{vdw}	ΔG_{essolv}	$\Delta G_{\text{nessolv}}$	$\Delta E_{\text{tot_ele}}$	ΔG_{bind}
WT	785.83(5.89)	$-98.12(0.46)$	$-711.52(5.24)$	$-15.95(0.04)$	$74.31(0.94)$	$-39.77(0.72)$
$L^{12}G$	742.63(4.21)	$-97.72(0.47)$	$-663.27(4.06)$	$-15.82(0.04)$	$79.36(0.63)$	$-34.18(0.49)$
$F^{25}E$	1205.06(4.54)	$-92.15(0.38)$	$-1122.28(4.34)$	$-15.55(0.04)$	$82.78(0.52)$	$-24.91(0.45)$
$F^{25}G$	876.20(4.10)	$-91.79(0.44)$	$-788.4(3.88)$	$-15.38(0.04)$	$87.8(0.57)$	$-19.37(0.48)$
$F^{25}L$	761.01(6.01)	$-95.57(0.40)$	$-683.93(5.6)$	$-15.88(0.04)$	$77.08(0.69)$	$-34.37(0.66)$
$Y^{84}G$	695.54(3.37)	$-76.71(0.26)$	$-644.68(3.20)$	$-14.63(0.03)$	$65.49(0.37)$	$-25.85(0.33)$
duplicates						
WT	761.56(3.32)	$-94.24(0.31)$	$-709.22(3.18)$	$-15.68(0.03)$	$68.02(0.45)$	$-41.90(0.33)$
$F^{25}G$	925.03(2.85)	$-89.58(0.25)$	$-858.26(2.66)$	$-15.02(0.03)$	$81.79(0.40)$	$-22.81(0.38)$
$Y^{84}G$	841.76(2.78)	$-82.9(0.32)$	$-784.02(2.59)$	$-14.89(0.03)$	$72.62(0.40)$	$-25.17(0.32)$

^a All values are in kcal/mol. Standard error of mean of each term is given in parentheses.

Myc-tagged wild type and mutant 14-3-3 σ proteins were similarly expressed and all wild type and mutant Flag-tagged proteins are efficiently immunoprecipitated by Flag antibody as determined by Western blot analysis of total lysate or immunoprecipitates. However, the amount of coimmunoprecipitated Myc-tagged mutant proteins were considerably less than that of the wild type with an order of wild type > $L^{12}G$ > $Y^{84}G$ > $F^{25}G$. Thus, these mutations clearly destabilize 14-3-3 σ homodimer formation with an order consistent with that of computational analyses.

Wild Type Has a Stable and Highly Packed Interfacial Core, Which Is Not Seen in $F^{25}G$ Mutant. To investigate how the above mutations affect 14-3-3 σ dimerization, we determined the potential effect of $L^{12}G$, $F^{25}G$, and $Y^{84}G$ mutations on the dimeric interfacial core. For this purpose, RMSD values of all atoms of interfacial core residues were calculated and compared between wild-type and mutant proteins. As shown in Figure 3B,C and Table 2, RMSDs of the core residues in both subareas of the

wild type have low standard deviations, indicating a stable structure. In contrast, the standard deviations of RMSDs of all mutants are higher, with $F^{25}G$ mutant the highest. We further determined the structural stability of the two interfacial cores by calculating the root-mean-square fluctuation (RMSF). As shown in Figure 3D, the average RMSF of core residues in wild type and $L^{12}G$, $F^{25}G$, and $Y^{84}G$ mutants were 0.44, 0.46, 0.54, and 0.49 Å, respectively. The RMSF of most core residues in wild type are below 0.5 Å, indicating very stable and solid-like interfacial cores.²⁵ RMSFs of all core residues in $F^{25}G$ are higher than that in wild type, reflecting more liquid-like cores according to Lindermann criterion.²⁶ Interfacial core residues in $L^{12}G$ and $Y^{84}G$ mutants also fluctuate more than that in the wild type, but less than that in the $F^{25}G$ mutant.

Hydrophobic Interfacial Core of Wild-Type Protein Is Protected from Water Penetration. We next investigated the effect of mutations on interfacial cores in their ability to repel water penetration. To determine the water exchange rate at interfacial

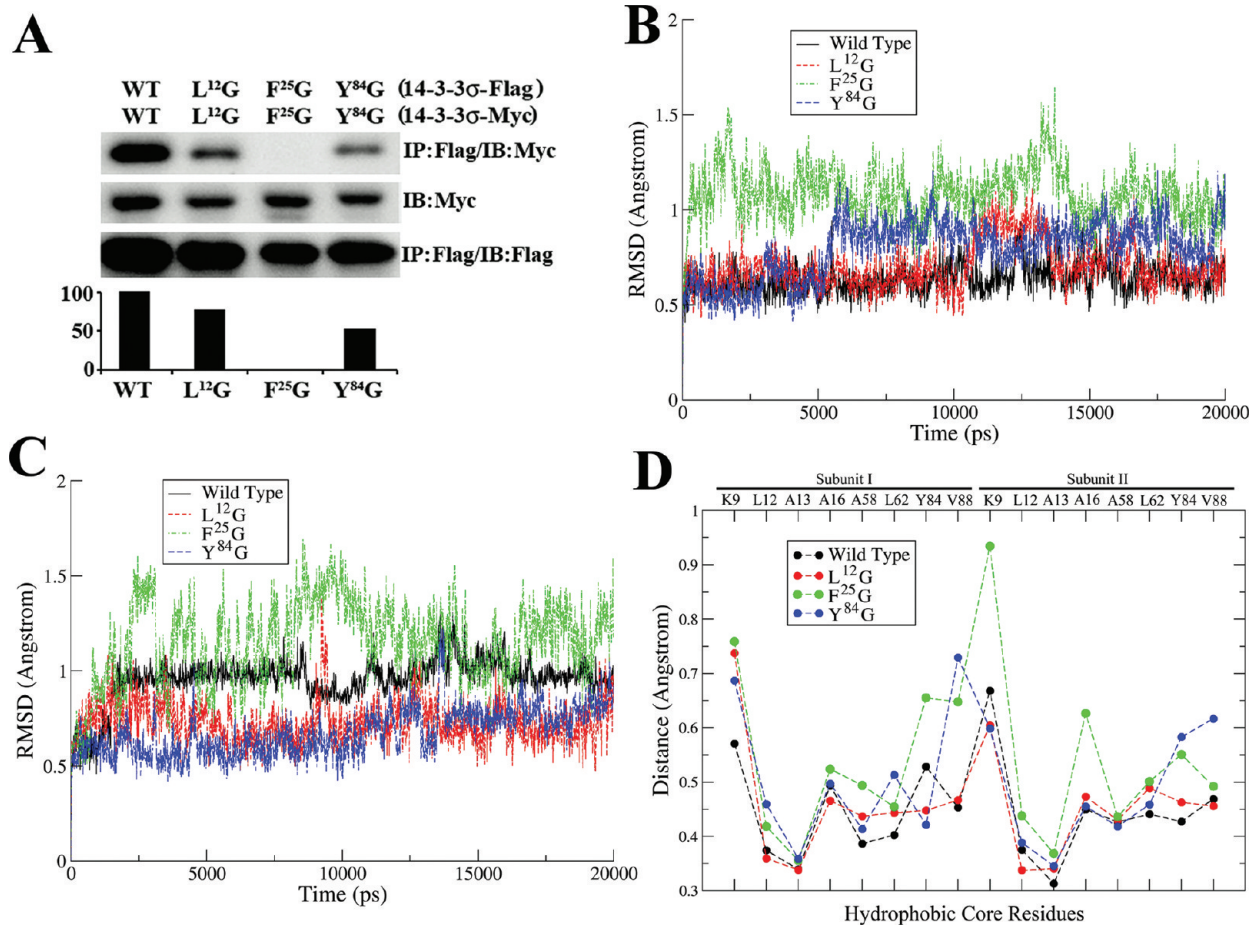


Figure 3. (A) Co-immunoprecipitation. MiaPaCa-2 cell lines with stable expression of Flag-tagged wild-type or mutant 14-3-3 σ were transiently transfected with myc-tagged wild type or mutant proteins, respectively, followed by immunoprecipitation with anti-Flag antibody and Western blot analysis using anti-Myc and anti-Flag antibodies. The coimmunoprecipitated myc-14-3-3 σ was quantified by determination of the band intensity using ScnImage software and normalization to their expression level as well as to the immunoprecipitation efficiency. (B) and (C) RMSD of all atoms of interfacial core residues in subarea I (B) and II (C). (D) RMSF of core residues in both subunits. Residue names are indicated at the top.

cores, a sphere of 6.0 Å in radius was drawn from the center of mass of the interfacial core residues at each subarea²⁷ (Figure 4A,B). Then, the number of water molecules moving in and out of the sphere every 200 ps was calculated for each subarea (Figure 4C–F). The average number of water molecules that move in and out of interfacial cores I and II in L¹²G, F²⁵G, and Y⁸⁴G mutants is higher than that in the wild type protein, with the F²⁵G mutant with the highest number (Table 4).

Role of Phe²⁵ in Stabilizing Interfacial Core via Interaction with Core Residues Tyr⁸⁴ and Lys⁹. The above studies showed that mutation of Leu¹², Phe²⁵, and Tyr⁸⁴ all reduced dimerization affinity of 14-3-3 σ and generated a more loosely packed interfacial core with higher water exchange rate compared with the wild-type protein. However, the F²⁵G mutation appears to have a greater effect on these properties than the other mutations. To determine how the F²⁵G mutation generates greater effects, we first tested if mutating Phe²⁵ to Gly²⁵ created a hole that resulted in a more water permeable core by monitoring the moving path of the water molecules found in the cores. As shown in Figure 4A,B, more water molecules move in and out of the cores of the F²⁵G mutant than of the wild-type protein. However, water does not seem to surge into the core solely by passing by Gly²⁵ in the F²⁵G mutant.

Rather, water enters and exits the sphere from different directions. Water molecules can penetrate the core via Val⁸⁸ and Glu⁹¹ of the opposite chain and residue Arg¹⁸, Lys⁹, and Asp²¹ on the same chain. These residues are far away from residue 25. Taken together with RMSD and RMSF analysis, we conclude that mutating Phe²⁵ into Gly²⁵ results in an overall loosely packed core and, thus, Phe²⁵ may play an important role in packing and stabilizing interfacial cores in favor of 14-3-3 σ dimerization.

We next investigated how mutating Phe²⁵ to Gly²⁵ unpacks the interfacial core. Analysis of the crystal structure reveals that Phe²⁵ makes contacts with interfacial residues located on both chains. Tyr⁸⁴, an interfacial core residue, is the only residue in the opposing chain that interacts with Phe²⁵. Consequently, we investigated the conformational stability of Tyr⁸⁴ on both chains in wild type and the L¹²G and F²⁵G mutants. Figure 5 shows the χ_1 and χ_2 dihedral angles of Tyr⁸⁴ during simulations. While the average χ_1 and χ_2 angles of Tyr⁸⁴ in wild type and the L¹²G mutant are comparable with similar standard deviation, indicating that Tyr⁸⁴ in these two structures has similar conformation and stability, the average χ_1 and χ_2 angles of Tyr⁸⁴ in the F²⁵G mutant vary between the two subunits with higher standard deviation, especially for χ_2 angles (Table 2). The higher standard deviation of χ_1 and χ_2 angles of Tyr⁸⁴ in the F²⁵G mutant

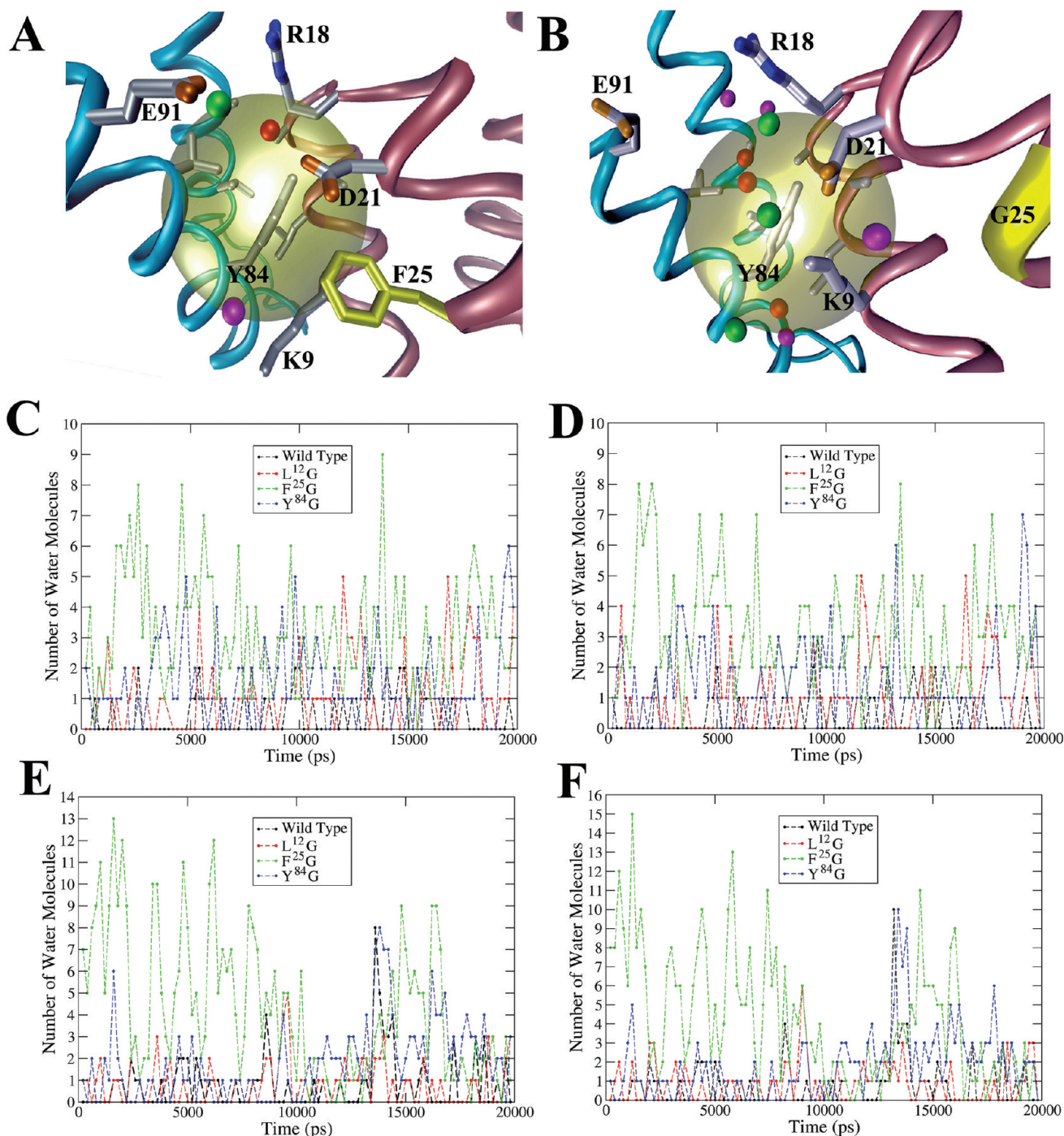


Figure 4. (A) and (B) A random simulation frame of wild type (A) and F²⁵G mutant (B) at subarea I of the dimeric interface. The sphere that is 6 Å in radius from the center of the mass of the interfacial core residues is depicted in yellow in transparency. Water molecules caught in the sphere are shown by red spheres. Compared with adjacent frames, water molecules moving toward and away the sphere are shown in magenta and green, respectively. Interfacial core residues are shown in gray. Residues that are engaged in strong hydrogen bonding across the dimeric interface are shown by atom type. Phe or Gly at position 25 in wild type (A) or F²⁵G (B) is labeled and colored in yellow. (C) and (D) Number of water molecules that move in (C) and out (D) of interfacial core I every 200 ps. (E) and (F) Number of water molecules that move in (E) and out (F) of interfacial core II every 200 ps.

suggests that Tyr⁸⁴ is more flexible in the F²⁵G mutant than in the wild type and the L¹²G mutant.

In addition to Tyr⁸⁴ in the opposing chain, several interfacial residues on the same chain also interact with Phe²⁵ as suggested by the crystal structure. Among them, Lys⁹ is the only residue located in the interfacial core. The conformational stability of

Lys⁹ in wild type and the mutants were thus examined. As shown in Figure 6A, B and Table 2, the χ_1 angle of Lys⁹ is similar among the wild type and the L¹²G and Y⁸⁴G mutants, but very different in the F²⁵G mutant. This observation indicates that the side chain of Lys⁹ in the F²⁵G mutant points to a different direction compared to the wild type and other mutants. In addition, the low

standard deviation suggests that this conformation of Lys⁹ in the F²⁵G mutant is stable and constant.

To compare the conformations of Lys⁹ in wild type and mutants, the average simulated structures of wild type and mutant proteins were aligned. As shown in Figure 6C, Lys⁹ in the wild type and the L¹²G and Y⁸⁴G mutants adopt a similar conformation in which the side chain of Lys⁹ extends across the dimeric interface and interacts with other core residues (Figure 6C). In the F²⁵G

mutant, however, with missing steric constraints from Phe²⁵, Lys⁹ turns and takes the space of Phe²⁵ and points to a direction away from the interfacial core. This new conformation of Lys⁹ is more exposed to solvent and loosens the highly packed interfacial core seen in wild type. Therefore, the bulky and stiff ring of Phe²⁵ in wild type 14-3-3 σ is critical in maintaining the rigidity of the interfacial core. This finding is consistent with the observed increase in RMSF of Lys⁹ in the F²⁵G mutant (Figure 3D).

Stability of Phe²⁵ Is Independent of Tyr⁸⁴ or Leu¹². We have shown that the F²⁵G mutation results in a more flexible ring of Tyr⁸⁴. We next tested if L¹²G or Y⁸⁴G mutation affects the stability of Phe²⁵ by examining χ_1 and χ_2 dihedral angles of Phe²⁵ in the wild-type and the L¹²G and Y⁸⁴G mutants. As shown in Supporting Information Figure S1C–F and summarized in Table 2, the average values and standard deviations of χ_1 and χ_2 angles in wild type and the L¹²G and Y⁸⁴G mutants are similar, suggesting that L¹²G or Y⁸⁴G mutation does not affect the conformation or stability of Phe²⁵ significantly. Therefore, Phe²⁵ is a stable residue independent of core residues Leu¹² and Tyr⁸⁴.

Role of Phe²⁵ in Maintaining Intermolecular Electrostatic Interactions. To investigate if L¹²G, F²⁵G, and Y⁸⁴G mutations affect intermolecular electrostatic interactions, hydrogen bonds that have at least 50% of occupancy between the two subunits of the 14-3-3 σ dimer during the simulation were determined and 5, 6, 2, and 3 hydrogen bonds are found in wild type and the L¹²G, F²⁵G, and Y⁸⁴G mutants, respectively (Table 5). The lowest number of hydrogen bonds found in the interface of the F²⁵G

Table 4. Average of Water Molecules That Move in and out Every 200 ps at the Hydrophobic Core of Each Subarea in Wild Type and Mutant 14-3-3 σ

	subarea I		subarea II	
	in	out	in	out
WT	0.46	0.46	0.80	0.80
L ¹² G	1.10	1.11	0.84	0.85
F ²⁵ G	3.21	3.19	4.32	4.19
Y ⁸⁴ G	1.50	1.54	1.83	1.84
F ²⁵ E	2.19	2.20	2.19	2.01
F ²⁵ L	0.77	0.74	1.19	1.21
	duplicates			
WT	0.39	0.39	0.79	0.78
F ²⁵ G	4.20	4.21	2.90	2.88
Y ⁸⁴ G	2.03	2.06	1.11	1.07

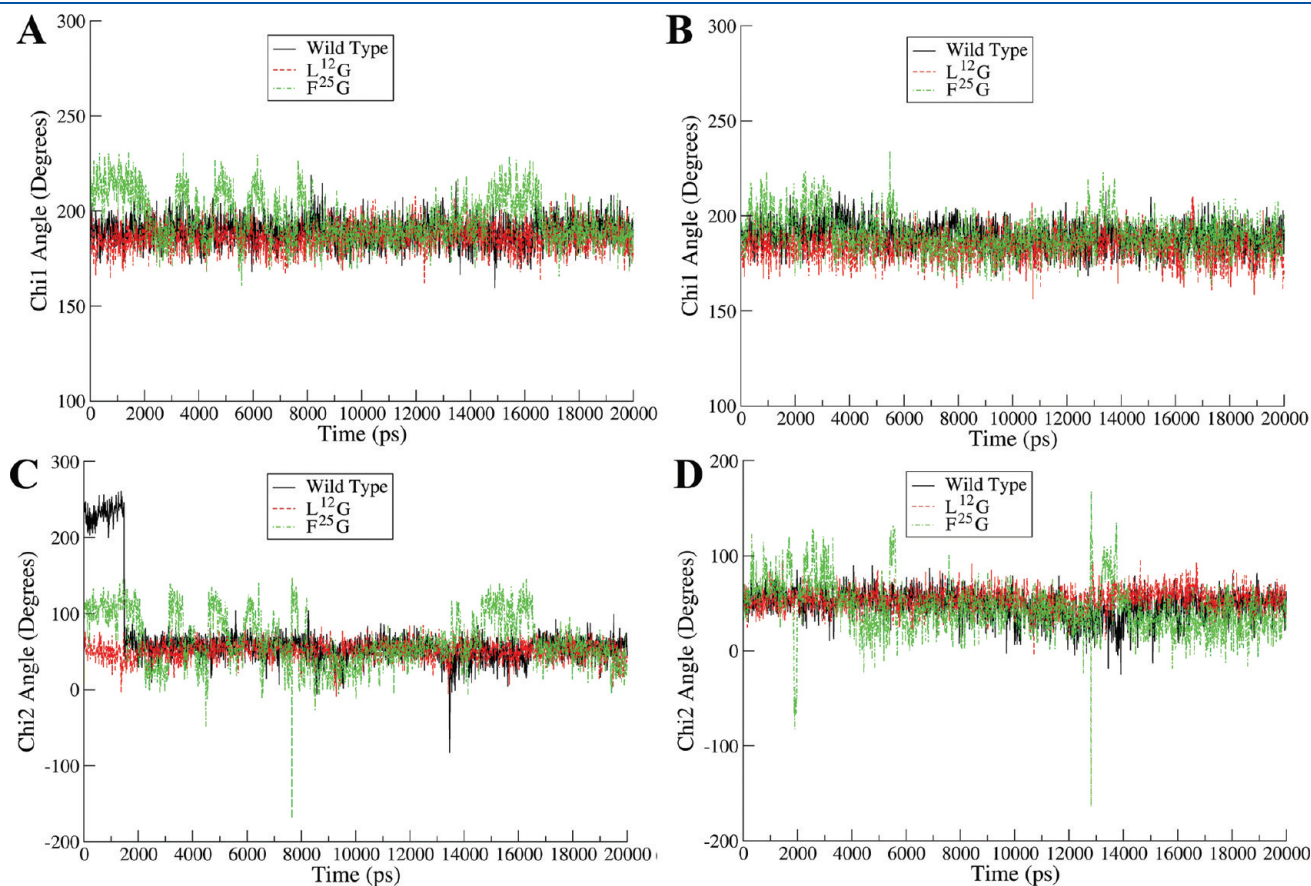


Figure 5. Side chain dihedrals of Tyr⁸⁴ in wild type and mutant 14-3-3 σ . χ_1 (A and B) and χ_2 (C and D) angles of Tyr⁸⁴ in subunit I (A and C) and II (B and D). χ_2 of Tyr⁸⁴ in subunit I of wild type (C) started at $\sim 233^\circ$ for the first 147 ps and then the single bond between atoms CB and CG turned 180° and was stabilized at the equivalent position of about 54° for the rest of the trajectory.

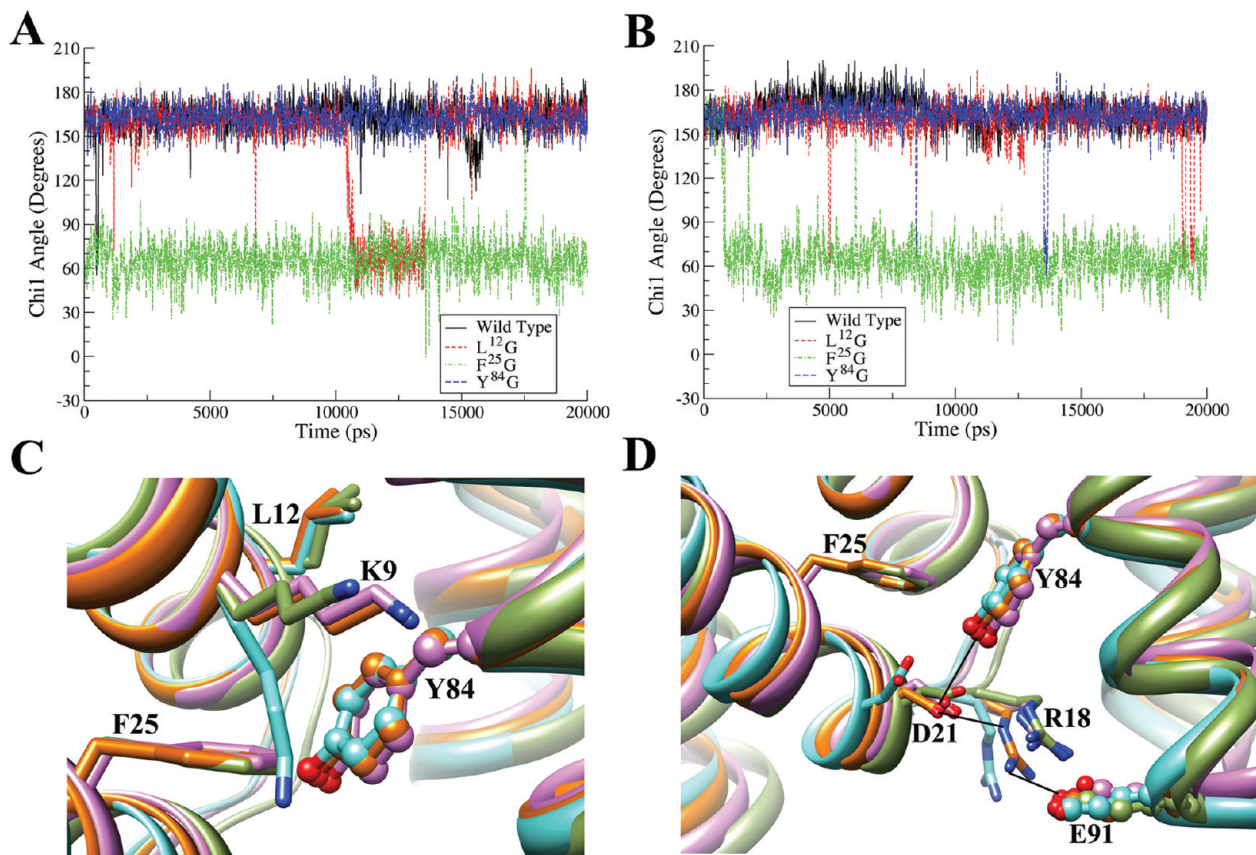


Figure 6. (A) and (B) χ_1 angle of Lys⁹ in subunit I (A) and II (B) in wild type, and L¹²G, F²⁵G, and Y⁸⁴G mutants of 14-3-3 σ . (C) and (D) Aligned average structure of wild type (orange), L¹²G (magenta), F²⁵G (cyan), and Y⁸⁴G (green) mutant 14-3-3 σ . Residue names are labeled as in wild type. Residues from one subunit are shown in stick representation and residues from the other subunit are shown in ball-and-stick representations.

mutant suggests that favorable electrostatic interactions between the two subunits are mostly disrupted.

Examination of the trajectories and average structures shows that Phe²⁵ stabilizes a hydrogen bond network (Figure 6D). In wild-type and the L¹²G and Y⁸⁴G mutants, the bulky and hydrophobic Phe²⁵ forces Asp²¹ to adopt a conformation that forms two hydrogen bonds, one with Tyr⁸⁴ on the opposing subunit and the other with Arg¹⁸ on the same chain. The second hydrogen bond helps orient Arg¹⁸ to hydrogen bond with the reciprocal Asp⁹¹ across the dimeric interface. The hydrogen bond between Arg¹⁸ and Asp⁹¹ could be important in associating the two monomers due to the close distance suggested by the crystal structure and due to the high occupancy suggested by our MD trajectories in all dimers except the F²⁵G mutant. In the F²⁵G mutant, however, the missing side chain of Phe²⁵ allows Asp²¹ to adopt a different conformation in which Asp²¹ interacts with solvent rather than with residues at the dimeric interface and thus destroys the hydrogen-bond network. As a result, the hydrogen bonds between Asp²¹ and Tyr⁸⁴ and between Arg¹⁸ and Glu⁹¹ have much lower occupancy in both subunits, which lead to a total loss of four hydrogen bonds in the F²⁵G mutant.

Duplicate Simulations. To confirm the above findings, we performed duplicate simulations of the wild type and the F²⁵G and Y⁸⁴G mutants. Similar to the original simulations, helices G, H and I are flexible while helices A, B, C and D are stable (Supporting Information Figure S2A,B, Table 6). F²⁵G loses its ability to stabilize the interfacial core (Supporting Information Figure S2C,D, Table 6). Lys⁹ in both subunits of F²⁵G turns and

adopts a different conformation than the other two trajectories (Supporting Information Figure S2E,F, Table 6). The order of total binding free energies of 14-3-3 σ dimers is wild type <Y⁸⁴G < F²⁵G (Table 3). In addition, lower binding free energies correspond to a higher water exchange rate at the interfacial cores (Supporting Information Figure S3A–D, Table 4). The missing side chain of Phe²⁵ in the F²⁵G mutant destabilizes Tyr⁸⁴ (Supporting Information Figure S4A–D, Table 6) while the missing side chain of Tyr⁸⁴ in Y⁸⁴G has no effect on Phe²⁵ (Supporting Information Figure S4E–H, Table 6). Finally, F²⁵G has smaller number of hydrogen bonds with low occupancy between the two 14-3-3 σ chains (Table 5). These observations show that the results observed in the original simulations are reproducible.

Essential Properties of Phe²⁵ for Its Critical Role at Dimeric Interface. The above findings suggest that the half-exposed Phe²⁵ is very important in packing the interfacial core of the 14-3-3 σ homodimer and in promoting both hydrophobic and electrostatic interactions favorable for dimer formation. To determine what properties of Phe²⁵ are crucial for dimer formation, we created two more virtual mutants by changing Phe²⁵ to Glu²⁵ (F²⁵E), which has a charged but large side chain comparable in size to Phe²⁵, and to Leu²⁵ (F²⁵L), which has similar hydrophobicity and bulkiness as Phe, but not as rigid. We then performed MD simulations and calculated the binding free energies of these mutants.

As shown in Table 3, the F²⁵E mutation generates significant changes to the electrostatic terms, which has the opposite effect in vacuum and solvent. Consequently, the F²⁵E mutant has a more favorable total binding free energy than the F²⁵G mutant.

Table 5. Occupancy of Hydrogen Bonds between the Two Subunits of Wild Type and Mutant 14-3-3 σ Dimers

	subunit I	subunit II	occupancy
wild type	GLU91	ARG18	91%
	ARG18	GLU91	83%
	TYR84	ASP21	65%
	SERS	GLU80	60%
	ASP21	TYR84	52%
L ¹² G	GLU91	ARG18	72%
	ARG18	GLU91	68%
	TYR84	ASP21	65%
	GLU80	SERS5	65%
	ASP21	TYR84	63%
F ²⁵ G	SERS	GLU80	55%
	SERS	GLU80	83%
	GLU80	SERS	71%
	ARG18	GLU91	139% ^a
	GLU91	ARG18	101% ^a
Y ⁸⁴ G	SERS	GLU80	61%
	GLU91	ARG18	126% ^a
	ARG18	GLU91	83%
	F ²⁵ E	GLU91	85%
	TYR84	ASP21	50%
duplicates			
WT	ARG18	GLU91	109% ^a
	GLU91	ARG18	106% ^a
	ASP21	TYR84	63%
	SERS	GLU80	55%
	TYR84	ASP21	53%
F ²⁵ G	GLU91	ARG18	75%
	GLU80	SERS	65%
	ARG18	GLU91	60%
	TYR84	ASP21	56%
	Y ⁸⁴ G	GLU91	131% ^a
GLU91			
ARG18			

^a An occupancy higher than 100% indicates that there are two hydrogen bonds between these two specified residues at certain moment.

The F²⁵L mutation further increases the affinity between the two subunits. These findings suggest that both the hydrophobicity and bulkiness of Phe²⁵ are important properties for its function in organizing the interfacial core and electrostatic interactions in the dimeric interface of 14-3-3 σ .

To validate the above findings, we engineered these new mutants and coexpressed differentially tagged proteins followed by coimmunoprecipitation analysis as described above. As shown in Figure 7A, while the F²⁵G mutation largely eliminated homodimeric 14-3-3 σ , the F²⁵E mutation retained ~20% of homodimers compared to the wild type protein. The F²⁵L mutation further increased the formation of homodimeric 14-3-3 σ to ~70% of the wild type protein. Thus, we conclude that both the hydrophobicity and bulkiness of Phe²⁵ are important properties for its function.

We further examined the average structures of these two newly generated mutants to determine how dimerization activities were

recovered in comparison with the F²⁵G mutant. As shown in Figure 7B, the large side chains of Glu and Leu at position 25 are able to restrain Lys⁹ in a conformation similar to that found in wild type. These two mutants also retain water resistance in the hydrophobic interfacial cores. The water exchange rate in F²⁵E and F²⁵L is lower than in F²⁵G, suggesting that the interfacial cores in F²⁵E and F²⁵L are more water resistant than in F²⁵G (Table 4, Figure 7C–F). The water exchange rate in F²⁵L is close to that in the wild type, suggesting that the hydrophobic property of the residue at position 25 is critical in organizing and protecting the interfacial core from water attacks. In addition, Asp²¹ in the F²⁵E and F²⁵L mutants adopts a conformation similar to the wild-type protein, helping to restore the hydrogen bond between Arg¹⁸ and Glu⁹¹ that is disrupted in the F²⁵G mutant (Table 5).

DISCUSSION

In this work, we used 14-3-3 σ as a homodimeric model protein and investigated several key residues at the dimeric interface that may play essential roles in homodimerization. We found that the interfacial core of a stable homodimer is devoid of water molecules and is dynamically stable and highly packed. Mutation of interfacial core residues which are usually conserved and deeply buried in the dimeric interface greatly compromises the affinity between the two subunits of 14-3-3 σ . Surprisingly, mutation of half-exposed and half-buried Phe²⁵ most dramatically suppressed the dimerization activity of 14-3-3 σ . Phe²⁵ plays a more important role in promoting 14-3-3 σ homodimerization by organizing both favorable hydrophobic and hydrophilic interactions. These findings suggest that residues at the interface play different roles other than providing a hydrophobic surface in the dimerization process, and provide a mechanism for how critical residues regulate others in favor of homodimerization.

The crystal structures of apo and ligand-bound 14-3-3 σ have a similar closed conformation.^{12,15} Our MD simulation studies show that without restraints from the phosphopeptide ligand, top helices G, H and I are flexible and can slide relative to the bottom helices. This dynamic motion of helices G, H and I resulting in the transition between closed and open conformations of apo-14-3-3 σ may be fundamentally important for 14-3-3 σ function in searching, recognizing and binding its protein partners since these helices are known to be involved in 14-3-3 σ ligand binding. This possibility is supported by the finding that in the crystal structure of apo 14-3-3 β (PDB code: 2BQ0), one subunit is in the open conformation while the other is in the closed conformation.²⁸ The observation of the closed conformation of the apo 14-3-3 σ crystal structure could be generated and stabilized by crystal packing.¹⁵ It is noteworthy that the conformational transition in top layer helices does not affect bottom helices engaged in dimerization and, thus, does not affect dimerization affinity.

It has been reported that residues at the dimeric interface do not contribute equally to dimerization as determined by systematic alanine scanning mutagenesis. A residue is defined as hot spot residue if its substitution by an Ala residue causes a loss of binding free energy of >2 kcal/mol.¹⁰ It has also been shown that hot spot residues are usually conserved and deeply buried.¹¹ In the case of 14-3-3 σ , Leu¹² and Tyr⁸⁴ are conserved residues in the 14-3-3 protein family and are deeply buried in the dimeric interface. These two residues provide the most buried surface area in the dimeric interface and contribute to the hydrophobic property of the interfacial core. Mutation of Leu¹² and Tyr⁸⁴ to Gly each greatly compromises the dimerization affinity of 14-3-3 σ .

Table 6. Average Standard Deviations of RMSDs and Dihedral Angles

properties	WT	F ²⁵ G	Y ⁸⁴ G	
overall Main Chain RMSD ± S.D. ^a	4.31 ± 1.88	3.34 ± 0.82	3.03 ± 0.75	
main chain RMSD ± S.D. ^a (Res. 1–107)	1.58 ± 0.30	1.56 ± 0.24	1.73 ± 0.44	
distance ^b between helices ABCD (Å)	19.32 ± 0.32	19.85 ± 0.35	19.76 ± 0.26	
distance ^b between helices GHI (Å)	68.51 ± 8.00	66.73 ± 3.26	65.47 ± 2.12	
all atoms RMSD of hydrophobic core residues ± S.D.	subarea I subarea II	0.81 ± 0.09 0.73 ± 0.08	1.20 ± 0.25 1.47 ± 0.26	0.84 ± 0.10 0.96 ± 0.12
χ ¹ ^c of Lys ⁹ ± S.D.	subunit I subunit II	147 ± 33 158 ± 16	69 ± 21 64 ± 24	162 ± 14 161 ^d ± 9
χ ¹ ^c of Phe ²⁵ ± S.D.	subunit I subunit II	169 ± 9 169 ± 8		172 ± 8 168 ± 8
χ ² ^c of Phe ²⁵ ± S.D.	subunit I subunit II	131 ± 12 131 ± 10		132 ± 11 132 ± 12
χ ¹ ^c of Tyr ⁸⁴ ± S.D.	subunit I subunit II	188 ± 8 192 ± 9	191 ± 8 198 ± 13	
χ ² ^c of Tyr ⁸⁴ ± S.D.	subunit I subunit II	56 ± 12 56 ± 12	41 ± 55 68 ± 35	

^a S.D. = standard deviation. ^b Distances are in angstrom. ^c Dihedrals are in degrees. ^d Data from 500 ps to 2 ns were used.

Therefore, these two residues are likely hot spot residues. Phe²⁵, however, is neither conserved nor deeply buried and, thus, does not qualify to be a hot spot residue. Yet, mutation of Phe²⁵ to Gly more dramatically reduces homodimerization of 14-3-3 σ . Interfacial core residues and electrostatic interactions in the dimeric interface become disorganized and disrupted in the absence of Phe²⁵. Phe²⁵ does not simply function as a gate-keeper that protects the interfacial core and favorable electrostatic interactions from water attack. Instead, it appears to promote and assemble co-operativity of critical residues at the dimeric interface in favor of dimer formation.

Phe²⁵ is an interesting and unique residue in 14-3-3 σ . The unique features including its physical location, rigidity, size, and hydrophobicity, all possibly contribute to its organizing function. Phe²⁵ has about half of its surface area exposed and half buried in the dimeric interface. This half-exposed and half-buried property of Phe²⁵ may provide an environment for its dual functions of organizing and regulating both hydrophobic and electrostatic interactions. Being outside of the interfacial core could be a requirement for Phe²⁵ in order to regulate and bestow stability to interfacial core residues. In addition, the finding that the conformation of Phe²⁵ is not affected in the L¹²G and Y⁸⁴G mutants suggests that Phe²⁵ may be a stable residue itself and its stability may not depend on other residues in the interfacial core. The stability or rigidity of Phe²⁵ may provide a strong anchor to force core residues to adopt specific conformations for dimerization. The finding of dimerization activity in the order of wild type > F²⁵L > F²⁵E > F²⁵G further suggests that the size and hydrophobicity of the side chain of Phe²⁵ are two important elements in organizing 14-3-3 σ dimerization.

The unique residue Phe²⁵ distinguishes the interfacial core of 14-3-3 σ from other 14-3-3 isoforms in two aspects. First, Phe²⁵ forms the unique aromatic pair with the conserved residue Tyr⁸⁴. Second, Phe²⁵ forces Lys⁹ adopt a conformation unique to 14-3-3 σ . Aromatic pairs had been frequently found at homodimeric interfaces.³ The Phe²⁵-Tyr⁸⁴ pair is unique to 14-3-3 σ and residues with smaller side chains are found at the same position of Phe²⁵ for all other 14-3-3 isoforms although they all have the conserved

Tyr⁸⁴. This unique property of 14-3-3 σ may contribute to its ability in strictly forming homodimers. It has been shown previously that 14-3-3 σ loses its preference of forming homodimers if three residues including Phe²⁵ (S⁵E, E²⁰D, and F²⁵C) are mutated simultaneously and mutating five residues including Phe²⁵ (S⁵E, E²⁰D, F²⁵C, Q⁵⁶R, E⁸⁰M) leads to 14-3-3 σ favoring hetero- instead of homodimerization.²⁹ These previous observations are consistent with our finding that mutating Phe²⁵ to a residue with a smaller side chain greatly reduces its ability to form homodimers. Furthermore, the unique conformation adopted by Lys⁹ in wild type 14-3-3 σ , due to the presence of the large and stiff hydrophobic side chain of Phe²⁵, may also contribute to the preference of homodimerization of 14-3-3 σ . Lys⁹ in the F²⁵G mutant adopts a different conformation than in the wild type, but is similar to the equivalent residue in other 14-3-3 isoforms such as Lys⁹ in 14-3-3 ζ (PDB code: 2V7D), Lys¹¹ in 14-3-3 β (PDB code: 2BQ0) or Arg⁹ in 14-3-3 η (PDB code: 2C63).²⁸ However, these isoforms, unlike 14-3-3 σ which strictly forms homodimers, have no preference for forming homo- or heterodimers. More interestingly, Lys¹² in 14-3-3 ϵ (PDB code: 2BR9),²⁸ which is more readily to form heterodimer, is located on a different side of helix A and is completely exposed to solvent. Thus, we conclude that Phe²⁵ may play a critical role in 14-3-3 σ homodimerization by organizing a unique interfacial core that favors homodimer, rather than heterodimer, formation. However, it is noteworthy that a single homodimeric protein is studied as a model protein here and it is not yet clear if a similar mechanism occurs in other homodimeric proteins. A future study of additional homodimeric proteins will help address this issue.

Identifying a biologically relevant unit of a protein complex in X-ray crystallography can be difficult due to crystal packing.^{3–5} To differentiate these two types of interactions, various studies have been performed. Chemical properties such as buried surface areas, nonpolar fraction of interface, and residue compositions of interface residues³⁰ were compared between interfaces in true dimers and “crystal” dimers. Other properties such as hydrophobic patches³¹, hydration of interfaces³² and conservations of

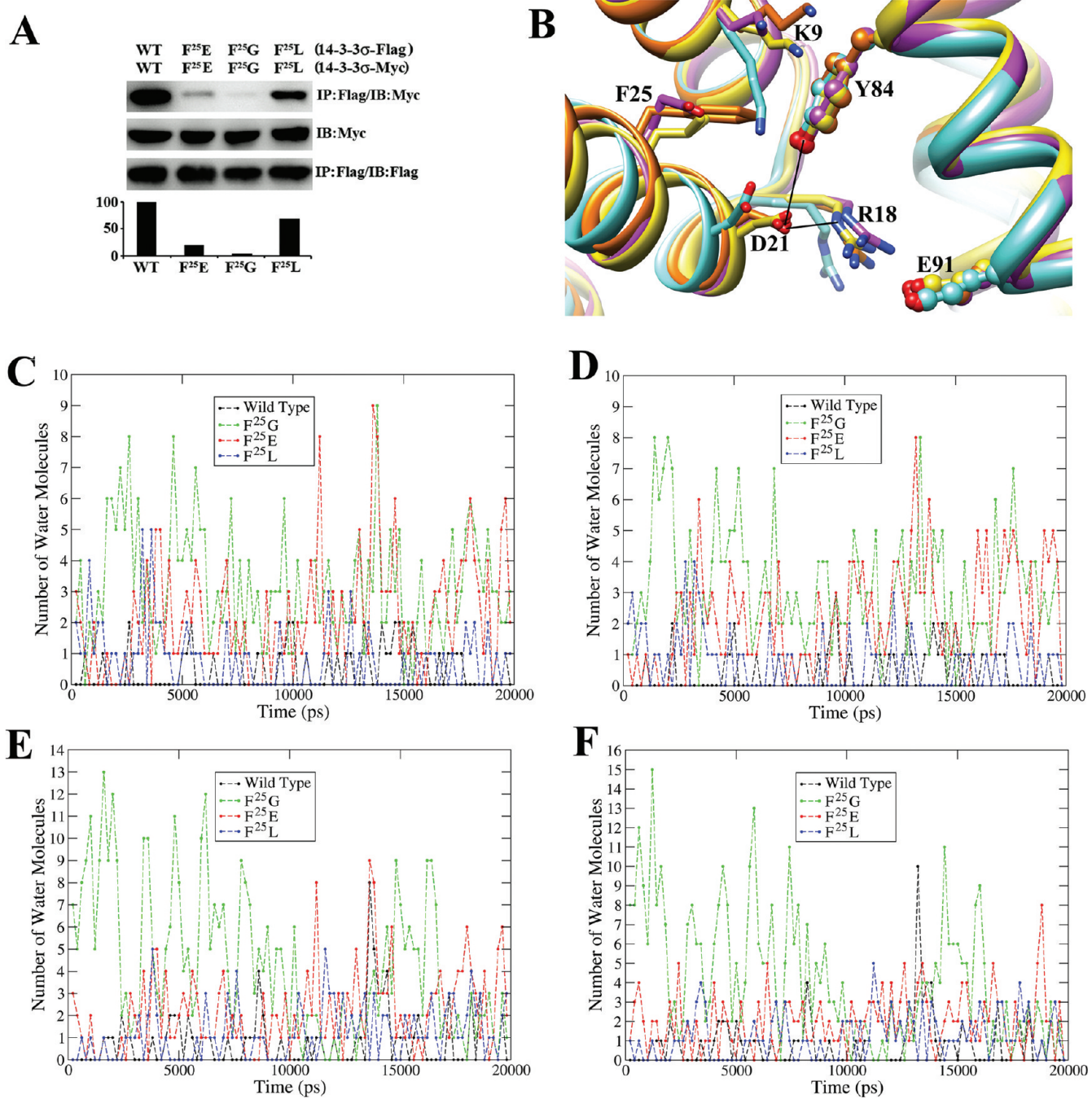


Figure 7. Properties of Phe²⁵ for its function in 14-3-3 σ dimerization. (A) Co-immunoprecipitation. MiaPaCa-2 cell lines with stable expression of Flag-tagged wild type or mutant 14-3-3 σ were transiently transfected with the same Myc-tagged constructs, followed by immunoprecipitation with anti-Flag antibody and Western blot analysis with anti-Flag and anti-Myc antibodies as described in Figure 3A. (B) Aligned average structure of wild type (orange), F²⁵G (cyan), F²⁵E (magenta) and F²⁵L (yellow). Lys⁹ and Asp²¹ in F²⁵E and F²⁵L mutants adopt conformations similar to those in the wild type and different from those in F²⁵G. The hydrogen bond network is restored in F²⁵E and F²⁵L. Residue names are labeled as in wild type. Hydrogen bonds in wild type are shown by black lines. Residues from one subunit are shown in stick representation and residues from the other are shown in ball-and-stick representations. (C) and (D) Number of water molecules that move in (C) and out (D) of interfacial core I every 200 ps in wild type and the F²⁵G, F²⁵E and F²⁵L mutants. (E) and (F) Number of water molecules that move in (E) and out (F) of interfacial core II every 200 ps in wild type, F²⁵G, F²⁵E, and F²⁵L.

interfacial residues³³ have also been investigated. A Voronoi tessellation-based method that includes multiple parameters has been developed to discriminate crystallographic from biologically relevant protein–protein interactions.³ An algorithm called ProBiS that detects structurally similar protein binding sites by

local structural alignment has been recently developed to predict protein–protein, protein–small ligand and protein–DNA binding sites.^{34,35} While these studies have shown different level of successes in discriminating and predicting these two types of interactions, the critical properties required for a biologically

relevant dimer have not been identified. Because crystal structures, which are still snapshots of proteins, were used in these previous studies, dynamic properties of protein dimeric interfaces could not be investigated. However, the dynamic properties may be critical for biologically relevant dimers. In this work, we used 14-3-3 σ as a homodimeric model protein and investigated the dynamic properties of the dimeric interface of wild-type and mutant 14-3-3 σ by performing water explicit MD simulations. We defined the interfacial core as that consisting of most buried residues. More specifically, two interfacial cores that consists of 16 residues, which have >80% solvent exposed surface area buried in the dimeric interface, were investigated. We found that the change in the dynamic properties of the interfacial core caused by one amino acid substitution could be successfully detected by water explicit MD simulations. The dynamic property of a highly packed interfacial core that has low water exchange rate observed in the wild-type 14-3-3 σ , but not in the F²⁵G mutant which lost high dimerization activity and can represent nonspecific protein–protein interactions, could be a prerequisite for stable protein complexes. Therefore, our finding may provide a new direction that can discriminate specific protein–protein interactions from nonspecific ones.

■ ASSOCIATED CONTENT

S Supporting Information. Primers used for engineering mutant 14-3-3 σ constructs, examination of secondary structural stability of mutants, structural stability of residue Phe²⁵ in wild type and mutants and figures for duplicate runs. This material is available free of charge via the Internet at <http://pubs.acs.org>.

■ AUTHOR INFORMATION

Corresponding Author

*Tel: (317) 274-7645; Fax: (317) 274-1560; E-mail: jliu2@iupui.edu (J.-Y.L.). Tel: (317) 278-4503; Fax: (317) 274-8046; E-mail: jianzhan@iupui.edu (J.-T.Z.).

■ ACKNOWLEDGMENT

The authors wish to thank Dr. Yaoqi Zhou for useful discussion and proof reading of this manuscript. Thanks also go to Valerie Fako for proof reading of the revised version of this manuscript and IU Big Red supercomputers for the CPU time. This work was supported in part by NIH Grant R01 CA140582.

■ REFERENCES

- Jailkhani, N.; Chaudhri, V. K.; Rao, K. V. S. Regulatory Cascades of Protein Phosphatases: Implications for Cancer Treatment. *Anti-Cancer Agents Med. Chem.* **2011**, *11*, 64–77.
- Mitra, S.; Cheng, K. W.; Mills, G. B. Rab GTPases implicated in inherited and acquired disorders. *Semin. Cell Dev. Biol.* **2011**, *22*, 57–68.
- Bernauer, J.; Bahadur, R. P.; Rodier, F.; Janin, J.; Poupon, A. DiMoVo: A Voronoi tessellation-based method for discriminating crystallographic and biological proteinprotein interactions. *Bioinformatics* **2008**, *24*, 652–658.
- Chen, X. M.; Bhandari, R.; Vinkemeier, U.; Van Den Akker, F.; Darnell, J. E.; Kuriyan, J. A reinterpretation of the dimerization interface of the N-terminal Domains of STATs. *Protein Sci.* **2003**, *12*, 361–365.
- Nussinov, R.; Tsai, C. J. Preface, Protein–protein interactions: Principles and prediction. *Phys. Biol.* **2005**, *2*, 1.
- Jones, S.; Thornton, J. M. Principles of protein–protein interactions. *Proc. Natl. Acad. Sci. U. S. A.* **1996**, *93*, 13–20.
- Keskin, O.; Gursoy, A.; Ma, B.; Nussinov, R. Principles of protein–protein interactions: What are the preferred ways for proteins to interact? *Chem Rev* **2008**, *108*, 1225–1244.
- Tsai, C. J.; Lin, S. L.; Wolfson, H. J.; Nussinov, R. Studies of protein–protein interfaces: A statistical analysis of the hydrophobic effect. *Protein Sci.* **1997**, *6*, 53–64.
- Tsai, C. J.; Nussinov, R. Hydrophobic folding units at protein–protein interfaces: Implications to protein folding and to protein–protein association. *Protein Sci.* **1997**, *6*, 1426–1437.
- Bogdan, A. A.; Thorn, K. S. Anatomy of hot spots in protein interfaces. *J. Mol. Biol.* **1998**, *280*, 1–9.
- Keskin, O.; Ma, B. Y.; Nussinov, R. Hot regions in protein–protein interactions: The organization and contribution of structurally conserved hot spot residues. *J. Mol. Biol.* **2005**, *345*, 1281–1294.
- Wilker, E. W.; Grant, R. A.; Artim, S. C.; Yaffe, M. B. A structural basis for 14-3-3 sigma functional specificity. *J. Biol. Chem.* **2005**, *280*, 18891–18898.
- Aitken, A. Functional specificity in 14-3-3 isoform interactions through dimer formation and phosphorylation. Chromosome location of mammalian isoforms and variants. *Plant Mol. Biol.* **2002**, *50* (6), 993–1010.
- Aitken, A.; Baxter, H.; Dubois, T.; Clokie, S.; Mackie, S.; Mitchell, K.; Peden, A.; Zemlickova, E. Specificity of 14-3-3 isoform dimer interactions and phosphorylation. *Biochem. Soc. Trans.* **2002**, *30*, 351–360.
- Benzinger, A.; Popowicz, G. M.; Joy, J. K.; Majumdar, S.; Holak, T. A.; Hermeking, H. The crystal structure of the non-liganded 14-3-3 sigma protein: Insights into determinants of isoform specific ligand binding and dimerization. *Cell Res.* **2005**, *15*, 219–227.
- Fu, H. A.; Subramanian, R. R.; Masters, S. C. 14-3-3 proteins: Structure, function, and regulation. *Annu. Rev. Pharmacol. Toxicol.* **2000**, *40*, 617–647.
- Zoete, V.; Meuwly, M. Importance of individual side chains for the stability of a protein fold: Computational alanine scanning of the insulin monomer. *J. Comput. Chem.* **2006**, *27*, 1843–1857.
- Collaborative Computational Project, N., The CCP4 Suite: Programs for protein crystallography. *Acta Crystallogr. D* **1994**, *50*, 760–763.
- Liu, Y.; Yang, Y.; Qi, J.; Peng, H.; Zhang, J.-T. Effect of cysteine mutagenesis on the function and disulfide bond formation of human ABCG2. *J. Pharmacol. Exp. Ther.* **2008**, *326*, 33–40.
- Li, Z.; Dong, Z.; Myer, D.; Yip-Schneider, M.; Liu, J.; Cui, P.; Schmidt, C. M.; Zhang, J.-T. Role of 14-3-3sigma in poor prognosis and in radiation and drug resistance of human pancreatic cancers. *BMC Cancer* **2010**, *10*, 598.
- Han, B.; Xie, H.; Chen, Q.; Zhang, J. T. Sensitizing hormone-refractory prostate cancer cells to drug treatment by targeting 14-3-3sigma. *Mol. Cancer Ther.* **2006**, *5*, 903–912.
- Liu, Y.; Liu, H. L.; Han, B. G.; Zhang, J. T. Identification of 14-3-3 sigma as a contributor to drug resistance in human breast cancer cells using functional proteomic analysis. *Cancer Res.* **2006**, *66*, 3248–3255.
- Xu, J.; Peng, H.; Chen, Q.; Liu, Y.; Dong, Z.; Zhang, J.-T. Oligomerization domain of the multidrug resistance-associated transporter ABCG2 and its dominant inhibitory activity. *Cancer Res.* **2007**, *67*, 4373–4381.
- Onufriev, A.; Bashford, D.; Case, D. A. Modification of the generalized Born model suitable for macromolecules. *J. Phys. Chem. B* **2000**, *104*, 3712–3720.
- Zhou, Y. Q.; Vitkup, D.; Karplus, M. Native proteins are surface-molten solids: Application of the Lindemann criterion for the solid versus liquid state. *J. Mol. Biol.* **1999**, *285*, 1371–1375.
- Lindemann, F. A. The calculation of molecular vibration frequencies. *Eur. Phys. J. Z* **1910**, *11*, 609–612.
- Zhou, R. H. Free energy landscape of protein folding in water: Explicit vs. implicit solvent. *Proteins: Struct., Funct., Genet.* **2003**, *53*, 148–161.
- Yang, X.; Lee, W. H.; Sobott, F.; Papagrigoriou, E.; Robinson, C. V.; Grossmann, J. G.; Sundstrom, M.; Doyle, D. A.; Elkins, J. M. Structural basis for protein-protein interactions in the 14-3-3 protein family. *Proc. Natl. Acad. Sci. U. S. A.* **2006**, *103*, 17237–17242.

- (29) Verdoordt, B.; Benzinger, A.; Popowicz, G. M.; Holak, T. A.; Hermeking, H. Characterization of 14-3-sigma dimerization determinants. *Cell Cycle* **2006**, *5* (24), 2920–2926.
- (30) Janin, J.; Chothia, C. The Structure of Protein-Protein Recognition Sites. *J. Biol. Chem.* **1990**, *265*, 16027–16030.
- (31) Lijnzaad, P.; Argos, P. Hydrophobic patches on protein subunit interfaces: Characteristics and prediction. *Proteins: Struct., Funct., Genet.* **1997**, *28*, 333–343.
- (32) Rodier, F.; Bahadur, R. P.; Chakrabarti, P.; Janin, J. Hydration of protein–protein interfaces. *Proteins* **2005**, *60*, 36–45.
- (33) Elcock, A. H.; McCammon, J. A. Identification of protein oligomerization states by analysis of interface conservation. *Proc. Natl. Acad. Sci. U. S. A.* **2001**, *98*, 2990–2994.
- (34) Konc, J.; Janezic, D. ProBiS algorithm for detection of structurally similar protein binding sites by local structural alignment. *Bioinformatics* **2010**, *26*, 1160–1168.
- (35) Konc, J.; Janezic, D. ProBiS: A web server for detection of structurally similar protein binding sites. *Nucleic Acids Res.* **2010**, *38*, W436–W440.